PROCEEDINGS OF SCIENCE

SuperTIGER Ultra-Heavy Glactic Cosmic Ray Atmospheric Propagation Corrections and Validation

Nicole E. Osborn,[a,*] **Brian F. Rauch**[†,a] **and Wolfgang V. Zober**[a] **for the SuperTIGER Collaboration**

[a] *Department of Physics and McDonnell Center for the Space Sciences, Washington University, St. Louis, MO 63130 USA*

E-mail: n.osborn@wustl.edu, brauch@physics.wustl.edu, wzober@wustl.edu

The SuperTIGER (Super Trans-Iron Galactic Element Recorder) balloon-borne ultra-heavy Galactic cosmic-ray (UHGCR) detector had successful Antarctic flights in 2012 (55 days) and 2019 (32 days). Stratospheric float altitudes varied between ~120,000 – 130,000 ft, and measurements must be corrected for propagation through the residual ~ 0.5% atmosphere using an approach developed for the preceding TIGER instrument. Changes due to nuclear interactions are determined iteratively starting from assumed top of the atmosphere (TOA) elemental abundances from which instrument abundances are found by solving networks of equations for all elements with partial and total charge changing cross sections stepping through fine slabs of material and adjusting the TOA abundances after each run until the predicted instrument abundances match the flight measurements. Differential elemental atmospheric energy losses are corrected for using Geant4 simulations to find TOA minimum energies corresponding to the acrylic Cherenkov detector threshold (~350 MeV/nuc) and scaling TOA abundances corrected for nuclear interactions with the fraction of the integral energy spectrum for its TOA minimum energy, using the iron spectrum for the UHGCR. Top of instrument (TOI) abundance at each element is then obtained from using total charge changing cross section and scaled partial charge changing cross sections to propagate TOA abundance through the fine slabs of material.

38th International Cosmic Ray Conference (ICRC2023)
26 July - 3 August, 2023
Nagoya, Japan

*Speaker

†SuperTIGER supported by NASA under grant numbers NNX09AC17G, NNX14AB25G, NNX15AC23G, and 80NSSC20K0405 and the Peggy and Steve Fossett Foundation

PoS(ICRC2023)173

1. Introduction

The best measurements of the ultra-heavy Galactic cosmic rays (UHGCR), $_{30}$Zn and higher charge elements, with single-element resolution to-date have been made by the balloon-borne Super Trans-Iron Galactic Recorder (SuperTIGER) instrument [7, 8, 13, 14] that is over four times the size of the predecessor TIGER instrument [5, 10, 11]. The advantage of balloon instruments is the larger geometric acceptances that can be flown than by space missions, but balloon-altitude measurements must be corrected for propagation through the residual atmosphere above the balloon. These corrections include those for nuclear interactions and energy losses in the instrument and atmosphere to derive top of the atmosphere (TOA) elemental abundances. SuperTIGER is nearly as large an UHGCR detector as can be flown on existing stratospheric balloons, and there is tension between detector size and weight versus higher altitude and reduced atmospheric burden.

The UHGCR provide insight into the origins of the Galactic cosmic rays (GCR), how they are accelerated, and the nucleosynthetic sources of the heavy elements. In Fig. 1 the relative abundances of elements from $_1$H to $_{56}$Ba and $_1$H to $_{82}$Pb for GCR with energies of 2 GeV/nucleon are compared with the Solar System (SS) abundances [6] normalized to $_{14}$Si. These two samples of galactic matter are nominally consistent, with most of the differences accounted for through both cosmic ray spallation between the source and detection and by acceleration efficiencies. In the GCR we see that $_{26}$Fe is ~5×10^3 times less abundant than $_1$H, the UHGCR from $_{30}$Zn to $_{40}$Zr are ~10^5 times less abundant than $_{26}$Fe, and the heavier UHGCR are even more scarce still.

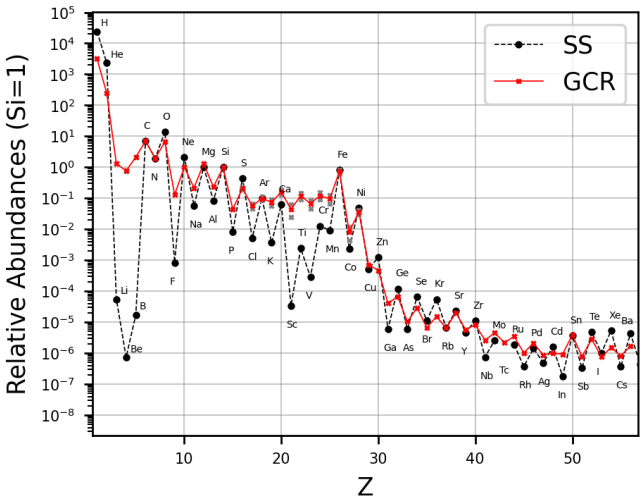

Figure 1: Solar System (SS) [6] and Galactic cosmic-ray (GCR) relative abundances at 2 GeV/nuc. Red line depicts average GCR data, sourced for 1≤Z≤2 from [12], Z=3 from [1], 4≤Z≤28 from [3], and 16≤Z≤56 from [13] normalized to $_{14}$Si. Grey dots depict overlapping measurements from [3] and [13].

2. SuperTIGER

2.1 Instruments

SuperTIGER is a supersized (~4×) version of the predecessor TIGER instrument. TIGER was a 1.16 m square 0.57 m tall stack of four compact wavelength-shifter readout scintillator detectors

sandwiching scintillating optical fiber hodoscopes above and below aerogel and acrylic Cherenkov light collection box detectors. One of two SuperTIGER modules is shown in Fig. 2a and in an expanded view in Fig. 2b, which is like two TIGER detectors connected together. SuperTIGER differs from TIGER in having only one scintillator at the top of the stack above the Cherenkov detectors to reduce the material in the GCR beam.

2.2 Flights

SuperTIGER had two successful Antarctic flights: SuperTIGER 2012 from December 8, 2012 - February 1, 2013 for 55 days with 5.38×10^6 $_{26}$Fe shown in Fig. 2c, and SuperTIGER 2019 from December 15, 2019 - January 17 2020 for 32 days with 1.3×10^6 $_{26}$Fe shown in Fig. 2d, where the UHGCR statistics scale with $_{26}$Fe. The first TIGER and SuperTIGER flights set duration records for zero-pressure heavy-lift stratospheric balloons, with the SuperTIGER record still standing.

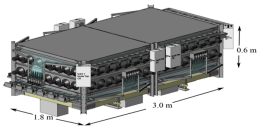

Figure 2(a): SuperTIGER module.

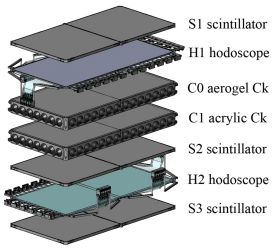

Figure 2(b): Expanded SuperTIGER module.

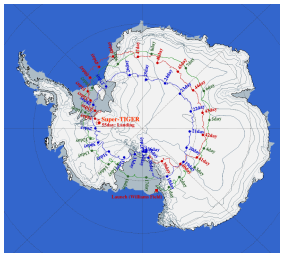

Figure 2(c): SuperTIGER 2012 flight.

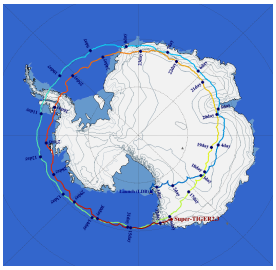

Figure 2(d): SuperTIGER 2019 flight.

3. Atmospheric Propagation Corrections

To compare GCR abundances measured in the instrument with measurements in space it is necessary to first correct the abundances for the interactions and energy losses as particles travel down through the atmosphere and within the instrument. Corrections are first made for the propagation in the instrument, and the material above the first charge detector (top scintillator) must be handled differently from that in the active region where interacting particles can be identified. The material at the top of the instrument is included in the atmospheric corrections that account for both loss and gain of each element through nuclear interactions, while within the active area of the detector only corrections for loss are made since interaction cuts have been applied. The inactive material above the top scintillator detectors was modeled with an equivalent depth of atmosphere in the propagation corrections, with 1.31 g/cm^2 for TIGER and 0.1 g/cm^2 for SuperTIGER based on the material above the top scintillator given in Table 2. Nuclear interaction probabilities and the rate of energy loss both increase for nuclei with higher Z, where energy loss increases as Z^2 and interactions increase with nuclear cross sectional area $\sim$A$^{2/3}$, where $A \propto Z$.

3.1 Cross Sections

TIGER and SuperTIGER cannot discriminate between isotopes, so the interactions considered in the atmospheric and instrument propagation corrections are total and partial charge changing cross sections. The total charge changing cross sections are used to correct for nuclear interaction losses

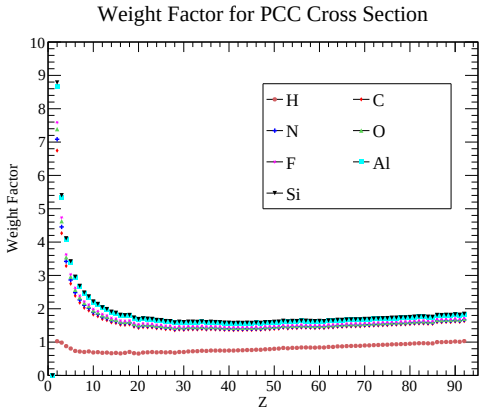

Figure 3(a): Partial charge changing cross section weight.

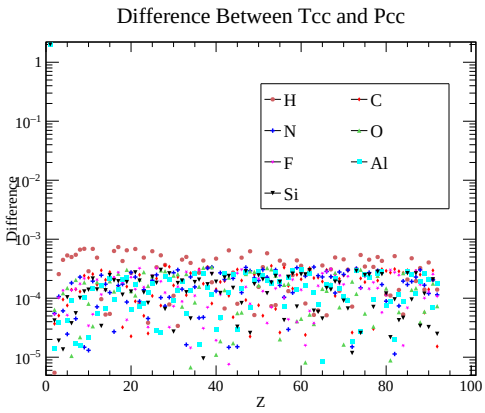

Figure 3(b): Difference between total charge changing cross section and partial charge changing cross section after the weight factor is added.

for each projectile element in the propagation. Partial charge changing cross sections correct nuclear interaction gains for each projectile element during the propagation. Each partial cross section is calculated at a ΔZ, a given charge change a projectile nuclei experiences. The sum of all partial charge changing cross sections, ΔZ, for a given projectile should equal to the total charge changing cross section.

The total charge changing cross sections are given by

$$\sigma_{tot}(P,T) = \pi[R_P + R_T - (3.20 \pm 0.05)]^2, \qquad (1)$$

where P and T refer to the projectile and target nuclei, and R_P and R_T are their respective nuclear radii. The nuclear radii have a hard sphere fitting parameter, S, that relates to the electron radii by $R_n = SR_e$. This parameter is S=1.277±0.006 with a χ^2 =5.59 [9]. This value was used in the calculation of R_P and R_T. The total charge changing cross sections are given in Fig. 4a for the materials used in the atmospheric propagation and instrument correction, showing the increase in the cross sections is less than linear in Z.

parameter	value
p_1	21.2 ± 0.5 mb
p_2	1.08 ± 0.15
p_3	(0.485 ± 0.014)A GeV
p_4	0.094 ± 0.013
p_5	1.11 ± 0.02
p_6	10.8 ± 1.6
p_7	(0.85 ± 0.03)A GeV
χ^2_ν	2.84
N	1741

Table 1: Partial charge changing cross section parameters taken from Table VIII in the paper [9].

The partial charge changing cross section is given by

$$\sigma_{\Delta Z}(A_P, A_T, K, \Delta Z) = p_1(A_P^{1/3} + A_T^{1/3} - p_2)(1 + p_3/K)|\Delta Z|^{-p_4[1+A_P^{1/3}/p_5+A_T^{1/3}/p_6+p_7/K]}, \qquad (2)$$

where A_P and A_T are the atomic masses of the projectile and target nuclei, ΔZ is the change in charge of the projectile, K is the total kinetic energy of the projectile, and the parameters are given in Table 1. For this analysis a value of $K = 2A$ GeV was selected as representative for the TIGER GCR and $K = 3.1A$ GeV was chosen for the SuperTIGER GCR. The total charge changing cross sections are shown in Fig. 4a for projectile targets in the atmosphere and material in the detector.

To ensure the total charge changing cross sections for a given charge equal the sum of the partial

charge changing cross sections, a weight factor to scale the partial charge changing cross sections was introduced. The weight factors are introduced after calculating the total charge changing cross section at each charge using Equation 1 and the sum of over ΔZ for each partial charge changing cross section from Equation 2. A multiplicative weight factor on the partial charge changing cross sections are varied until the weighted partial cross section equals the total cross section. The charge dependence of the weight factor given in Fig. 3a is non-linear in charge especially at low Z. The weight factor ensured the total and partial charge changing cross sections were within 1%, with the differences shown in Fig. 3b. These corrected factors produce total and partial charge changing cross sections for the projectile elements from $_{27}$Ni to $_{40}$Zr for the atmospheric gas targets of $_{7}$N and $_{8}$O as shown in Fig. 4b and Fig. 4c, respectively.

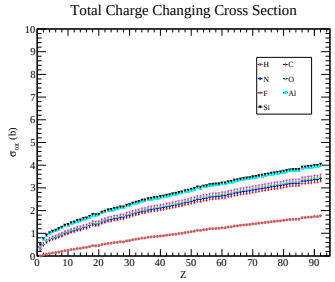

Figure 4(a): Total charge changing cross sections of projectile nuclei on target nuclei $_{1}$H, $_{6}$C, $_{7}$N, $_{8}$O, $_{9}$F, $_{13}$Al, and $_{14}$Si.

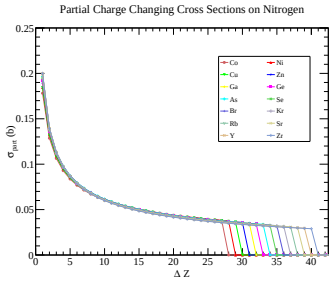

Figure 4(b): Partial charge changing cross sections on $^{14}_{7}$N for targets $_{27}$Co to $_{40}$Zr.

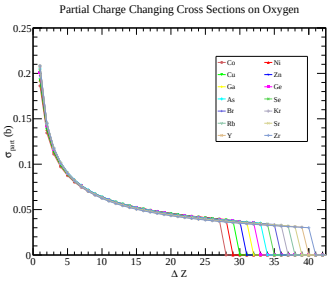

Figure 4(c): Partial charge changing cross sections on $^{16}_{8}$O for targets Z = $_{27}$Co to $_{40}$Zr.

3.2 Instrument and Energy Correction

The measured abundances are corrected to the top detector for interaction losses in the active instrument area in TIGER [5, 10, 11] and SuperTIGER [7, 8, 13]. Corrections for the inactive detector material above the middle of the top scintillator radiator in TIGER and SuperTIGER listed in Table 2 were folded into the corrections for interactions in the atmosphere. The top insulation for SuperTIGER is melamine ($C_3H_6N_6$) foam, but foam is polymerized malamine sodiumbisulfide ($C_9H_6Na_6S_6O_{18}$), which is presumed to lose H in polymer linkages, at least two per molecule to form a strand and more for cross linkages. To date this material has been approximated as acrylic.

A correction for energy losses is made by calculating the minimum energy at the top of the atmosphere required to be above threshold in the acrylic Cherenkov detector based on the average energy losses in detector materials and the atmosphere. The top of the atmosphere abundances corrected for interactions in the atmosphere are then renormalized compared to $_{26}$Fe based on evaluating the normalized integral spectrum of each element derived from differential spectra [4] for elements below $_{26}$Ni and scaled $_{26}$Fe spectra for UHGCR.

3.3 Propagation

In the atmosphere and instrument material, the correction process tracks the charge changing interactions that will add to or reduce the flux of each charge according the projectile and target nuclei. The total and partial charge changing cross sections are used to correct SuperTIGER measured abundances to TOA abundances. The TOA abundances in the model are assumed

detector material	chemical formula	TIGER top	TIGER active	ST top	ST active
PET	$C_{10}H_8O_4$	0.102	0	0.025	0.062
PMMA	$C_5H_8O_2$	0	0.938	0.040	1.499
aluminum	Al	0.148	0.07	0.033	0.372
PS	C_8H_8	0.342	1.920	0	0.388
PVT	C_9H_{10}	0.412	1.442	0.523	1.057
silica	SiO_2	0	0.586	0	0.614

Table 2: TIGER and SuperTIGER instrument materials above middle of first scintillator detector (top) and in average in the active area (active) in g/cm^2: polyethylene terephthalate (PET) - Mylar, polymethyl methacrylate (PMMA) - acrylic, aluminum (Al), polystyrene (PS), polyvinyltoluene (PVT), silica SiO_2.

First Step	Last Step	Difference
115600.8876	115168.5385	0.3747 %

Table 3: The total charge abundance at the first step of the iteration compared to the final step.

using satellite GCR measurements from HEAO-3-C2, HEAO-3-C3, and Ariel [2, 3]. The TOA abundances are iterated for n_{step}=1000 steps. The abundance of a projectile in a step i+1 of atmosphere is calculated using the abundance at step i by adjusting for the losses and gains due to nuclear interactions as $J_{i+1}(P) = J_i(P) - L_i(P) + G_i(P)$. The loss term is given by

$$L_i(P) = J_i(P)10^{-24}\frac{N_{atm}}{n_{step}}N_A\left(\sigma_{tot,N}(P,N)r_N + \sigma_{tot,O}(P,N)r_O\right), \tag{3}$$

where N_{atm} is the surface mole density of the atmosphere, N_A is Avogadro's Number, $\sigma_{tot}(P)$ is the total charge changing cross section for a projectile P on the target with r_N and r_O being the number fractions of Nitrogen and Oxygen in the atmosphere, respectively. The gain term which produces two daughter nuclei is given by

$$G_i(P) = \sum_{\Delta Z = Z(P') - Z(P) > 0}\left[J_i(P')10^{-24}\frac{N_{atm}}{n_{step}}N_A(\sigma_{\Delta Z,N}r_N + \sigma_{\Delta Z,O}r_O)\right], \tag{4}$$

where the sum is over ΔZ where the charge change of a projectile P' is greater than the charge of a projectile P and $\sigma_{\Delta Z}$ is the partial charge changing cross section of a projectile P' with a given ΔZ from interacting with a target nuclei $_7$N or $_8$O.

Charge must be conserved through the propagation. At each step the absolute abundance of each charge can be multiplied by the respective charge to confirm that during the propagation the charge is conserved. The TOA charge compared with the charge after propagation changes by less than 0.4%, see Table 3. The relative charge change after the propagation for each charge is seen in Fig. 5.

4. Results and Discussions

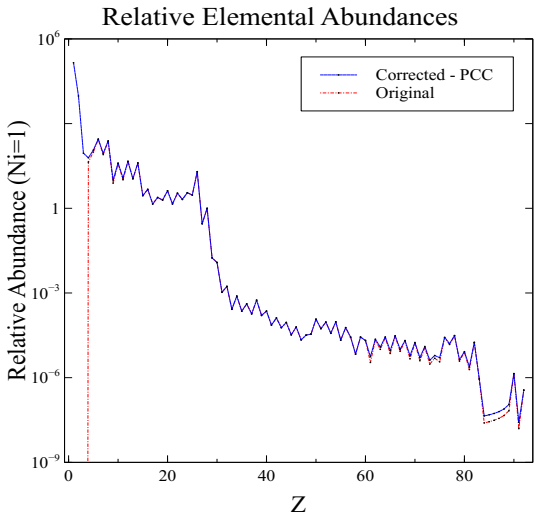

Figure 6(a): Relative abundances after scaling the partial charge changing cross sections (blue) compared with abundances without scaling the partial charge changing cross sections (red).

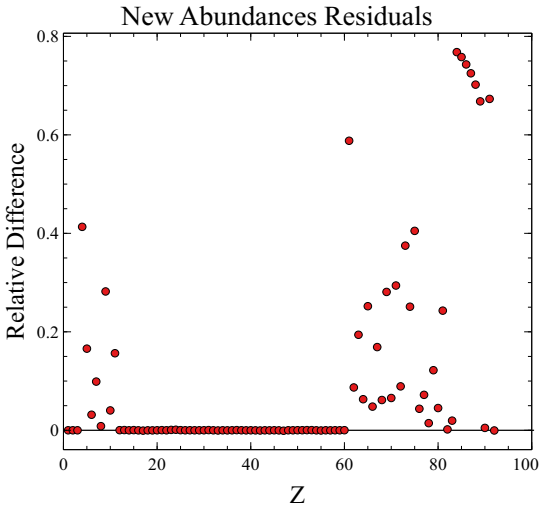

Figure 6(b): Difference between total and partial charge changing cross section after scaling the partial cross sections.

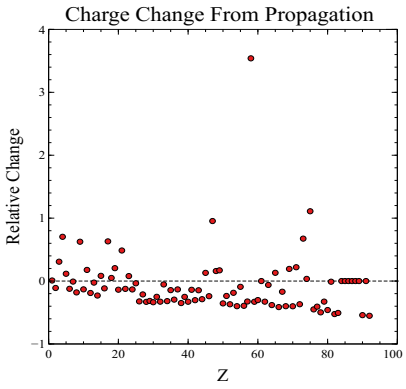

Figure 5: Relative change in charge between the initial and final step.

Atmospheric nuclear interaction corrections using the total and partial charge changing cross sections produce final abundances consistent with SuperTIGER raw abundances. Introducing a weight factor for the partial charge changing cross sections affects the propagation model leading to different final abundances compared to not scaling the partial cross sections. The final abundance from propagation after scaling the partial cross sections is compared to the propagation using unweighted partial cross sections in Fig. 6a. The most significant change were in Z = $_{4}$Be-$_{11}$Na and Z > $_{60}$Nd. The correction predominantly produced positive residuals seen in Fig. 6b. The abundances were higher from scaling that increased the partial charge changing cross sections which led to a larger $G_i(P)$ term in the step propagation, 4.

The next step in this analysis is to fully implement a MonteCarlo method to estimate systematic uncertainties by simultaneously and randomly varying atmospheric propagation total and partial charge changing cross sections over multiple trials to find a range of variation for TOA elemental abundances. Further down the line the goal is to use simulations for a more advanced model of nuclear interactions in the atmosphere.

5. Acknowledgements

The material contained in this document is based upon work supported by a National Aeronautics and Space Administration (NASA) grant or cooperative agreement. Any opinions, findings, conclusions, or recommendations expressed in this material are those of the author and do not necessarily reflect the views of NASA.

6. References

[1] M. Aguilar et al. Isotopic Composition of Light Nuclei in Cosmic Rays: Results from AMS-01. *The Astrophysical Journal*, 736(2):105, Aug. 2011.

[2] W. R. Binns, T. L. Garrard, P. S. Gibner, M. H. Israel, M. P. Kertzman, J. Klarmann, B. J. Newport, E. C. Stone, and C. J. Waddington. Abundances of Ultraheavy Elements in the Cosmic Radiation: Results from HEAO 3. , 346:997, Nov. 1989.

[3] J. J. Engelmann, P. Ferrando, A. Soutoul, P. Goret, E. Juliusson, L. Koch-Miramond, N. Lund, P. Masse, B. Peters, N. Petrou, and I. L. Rasmussen. Charge composition and energy spectra of cosmic-ray nuclei for elements from Be to Ni - Results from HEAO-3-C2. , 233:96–111, July 1990.

[4] J. S. George et al. Elemental Composition and Energy Spectra of Galactic Cosmic Rays During Solar Cycle 23. *The Astrophysical Journal*, 698(2), 2009.

[5] J. T. Link. *Measurements of Ultra-Heavy Galactic Cosmic Rays with the TIGER Instrument*. PhD thesis, Washington University in St. Louis, 2003.

[6] K. Lodders. Solar System Abundances and Condensation Temperatures of the Elements. *The Astrophysical Journal*, 519:1220–1247, 2003.

[7] R. P. Murphy. *Identifying the Origin of Galactic Cosmic Rays with the SuperTIGER Instrument*. PhD thesis, Washington University in St. Louis, 2015.

[8] R. P. Murphy et al. Galactic Cosmic Rays Origins and OB Associations: Evidence from SuperTIGER Observations of Elements ${}_{26}$Fe through ${}_{40}$Zr. *The Astrophysical Journal*, 831(2):148, 2016.

[9] B. S. Nilsen et al. Fragmentation Cross Sections of Relativistic ${}^{84}_{36}$Kr and ${}^{109}_{47}$Ag Nuclei in Targets From Hydrogen to Lead. *Physical Review C*, 52(6):3277–3290, 1995.

[10] B. F. Rauch. *Measurement of the Relative Abundances of the Ultra-Heavy Galactic Cosmic Rays ($30 \leq Z \leq 40$) with the Trans-Iron Galactic Element Recorder (TIGER) Instrument*. PhD thesis, Washington University in St. Louis, 2008.

[11] B. F. Rauch, J. T. Link, K. Lodders, M. H. Israel, L. M. Barbier, W. R. Binns, E. R. Christian, J. R. Cummings, G. A. de Nolfo, S. Geier, R. A. Mewaldt, J. W. Mitchell, S. M. Schindler, L. M. Scott, E. C. Stone, R. E. Streitmatter, C. J. Waddington, and M. E. Wiedenbeck. Cosmic Ray Origin in OB Associations and Preferential Acceleration of Refractory Elements: Evidence from Abundances of Elements ${}_{26}$Fe through ${}_{34}$Se. *The Astrophysical Journal*, 697(2):2083–2088, 2009.

[12] T. Sanuki et al. Precise Measurement of Cosmic-Ray Proton and Helium Spectra with the BESS Spectrometer. *The Astrophysical Journal*, 545(2):1135–1142, 2000.

[13] N. E. Walsh. *SuperTIGER Elemental Abundances for the Charge Range* $41 \leq Z \leq 56$. PhD thesis, Washington University in St. Louis, 2020.

[14] N. E. Walsh et al. SuperTIGER Abundances of Galactic Cosmic Rays for the Atomic Number (Z) Interval 30 to 56. In *Proceedings of 37th International Cosmic Ray Conference — PoS(ICRC2021)*, volume 395, page 118, 2021.

Full Author List: SuperTIGER Collaboration

Q. Abarr[1], Y. Akaike[2], W. R. Binns[1], T. J. Brandt[2], D. L. Braun[1], J. H. Buckley[1], N. W. Cannady[3,2,4], R. M. Crabill[5], G. A. de Nolfo[6], P. F. Dowkontt[1], S. P. Fitzsimmons[2], P. Ghosh[7,2,4], T. Hams[8], M. H. Israel[1], J. F. Krizmanic[2], W. Labrador[1], A. W. Labrador[5], L. Lisalda[1], R. A. Mewaldt[5], J. G. Mitchell[6], J. W. Mitchell[2], R. P. Murphy[1], S. Nutter[9], M. A. Olevitch[1], N. E. Osborn[1], B. F. Rauch[1], K. Sakai[3,2,4], M. Sasaki[10,2,4], F. S. Sebastian[2], G. E. Simburger[1], E. C. Stone[5], T. Tatoli[3,2,4], N. E. Walsh[1], J. E. Ward[1], A. T. West[1], M. E. Wiedenbeck[11], W. V. Zober[1],

[1]Department of Physics and McDonnell Center for the Space Sciences, Washington University in St. Louis, [2]NASA Goddard Space Flight Center, Astrophysics Science Division, [3]University of Maryland, Baltimore County, [4]Center for Research and Exploration in Space Sciences and Technology II, [5]California Institute of Technology, [6]NASA Goddard Space Flight Center, Heliophysics Science Division, [7]Catholic University of America, [8]NASA, [9]Northern Kentucky University, [10]University of Maryland, College Park, [11]NASA Jet Propulsion Laboratory,

PoS(ICRC2023)173